Synthesis Process and Structural Properties of Single and Mixed Hallide Sn-based Pervoskite Materials in Photovoltaic Application

Kanij Fatema[1,2,*], Farid Ahmed[1]

1Department of Physics, Jahangirnagar University, Savar, Dhaka-1342, Bangladesh
2Department of Electrical and Electronic Engineering, Bangladesh University of Business and Technology (BUBT), Dhaka-1216, Bangladesh
*Corresponding Author's Email: kanij_fatema@bubt.edu.bd

Abstract— Organic-inorganic perovskite solar cell is highly promising technology among all known photovoltaic technologies for its increasing power conversion efficiency, material abundance, low cost and simple synthesis technique. The perovskite materials mainly $CH_3NH_3SnCl_3$ (MASC) and $CH_3NH_3ISnCl_2$ (MAISC) are synthesized using chemical synthesis process as Sn-based perovskite materials because of its simplicity. The Sn-based perovskite materials have been characterized for structural properties and morphological structure by using technique X-ray diffraction (XRD) and scanning electron microscope (SEM). The MASC having cubic crystal phase (a=b=c & α = β = γ = 90°) and MAISC having tetragonal structure (a=b=c & α = β = γ = 90°) with average grain size are 40.9 nm and 40.62 nm The SEM structure shows some irregular crystal growth having average particle size ~ 334.68 μm for MASC and ~ 464.88 μm.

Index Terms— Perovskite, Sn-based, MASC, MAISC, XRD, SEM, Grain size

1 Introduction

Organic-inorganic perovskite solar cell is most efficient solar cell because of its higher power conversion, low cost and availability of compound in nature. The light absorbing perovskite materials are sandwiched between hole transport layer (HTL) and electron transport layer (ETL) and these two layers maintains air stability of perovskite materials [1][2]. The general compound formula of perovskite compound is ABX3, A is aliphatic or atomic ammonium and B is divalent metal cations such as Pb2+, Sn2+, Cu2+ etc. and X is the halogen such as Cl-, Br-, I- [3][4]. the most of the perovskite solar cells are focused on methylammonium lead trihalide (CH3NH3PbX3) and formamidinium lead trihalide (H2NCHNH2PbX3) as perovskite absorber where X= I-, Br-, Cl- [5]. The perovskite materials have been well known for many years but first incorporation into solar cell is reported in 2009, where 3.81% power conversion efficiency has been achieved [6]. The power conversion efficiency has been developed rapidly within 2 years and the long-term power conversion efficiency reached ~ 6.54% in 2011 using 2~3 nm sized perovskite (CH3NH3PbI3) nanocrystal [7]. Organic-inorganic perovskite solar cell consists of promising photoactive material in photovoltaic application for its higher power conversion efficiency and its outstanding optoelectronics properties, charge carrier mobility, charge carrier diffusion length and dielectric properties [8][9]. In 2015 Heo and Im reported ~18.3%-19% power conversion efficiency by varying thickness 500 nm ~900 nm for the hybrid perovskite structure (CH3NH3PbI3-XClx) [10]. According to NERL the perovskite solar cell has been achieved maximum power conversion efficiency 25.5% [11] in 2021.

Though lead-based perovskite solar cell achieved highest efficiency but toxicity of lead is major concerns. Among different perovskite structures, in replacement of lead ecofriendly Sn –based perovskite (CH3NH3SnX3) solar cell is new challenge for researcher in photovoltaic application because of its abundance in nature, environment friendly, ideal band gap and crystal structure similar to lead-based perovskite [12][13][14]. However, lead-free Sn-based halides perovskite absorbers have low toxicity, narrow direct band gaps, high optical-absorption coefficients, high mobilities, low exciton-binding energies, long charge-carrier life times and good stability. Therefore, Sn-based perovskite structure having attractive properties in photovoltaic application under standard operating conditions [15]. Lead free perovskite solar cell particularly using perovskite absorber CH3NH3SnI3 is achieved power conversion efficiency 6% with band gap 1.23 eV [16]. The Sn-based perovskite solar cell have been achieved 8.3% power conversion efficiency for fresh device [17]. Moreover, Nishimura et al., found the conversion efficiency of 13.24% by depositing the precursor on Florine doped tin oxide (FTO) substrate in 2020 [12].

Lead free tin-based perovskite materials CH3NH3SnCl3 (MASC) and CH3NH3ISnCl2 (MAISC) was synthesized for basic properties. Then the synthesized CH3NH3SnCl3 and CH3NH3ISnCl2 was characterized by using X-ray diffraction for structural properties and scanning electron microscopy for morphological structure. The Sn based perovskite absorber CH3NH3SnCl3 and CH3NH3ISnCl2 was synthesized using following procedure and characterized them.

2 Experimental Process

2.1 Reagents

CH3NH2 (40% mono) was purchased from Qualikems, HI

(67% in H2O), HCl (32% in H2O) and tin (II) chloride-2-hydrate were purchased from Merck.

2.2 Synthesis of CH3NH3I and CH3NH3Cl

The perovskite materials are synthesized using chemical method, vapor-assisted method, dual source evaporation method and sequential deposition method. Among these synthesis process chemical synthesis process is effective.

Methylamine (CH3NH2) was reacted with hydroiodic acid (HI) in 1:1 molar ratio. The three-arm flask was filled with CH3NH2 and HI was added dropwise with methylamine solution. The flask was put on ice bath and the methylammonium iodide (CH3NH3I) solution was kept 3 hours in ice bath. The CH3NH3I (MAI) solution was collected and evaporated at 60°C. After evaporation the crystalline (MAI) was washed several times by diethyl ether and dried.

Again, methylamine (CH3NH2) was reacted with hydrochloric acid (HCl) in 1:1 molar ratio. The flask was put on ice bath and the methylammonium iodide (CH3NH3Cl) solution was kept 3.10 hour in ice bath. The CH3NH3Cl (MAC) solution was collected and evaporated at 55 °C by using rotary evaporator. After evaporation, the crystalline MAC was washed several times by diethyl ether and dried crystal of MAC was collected [18]. Figure 1 shows the dried MAI and MAC.

Fig. 1. Synthesized (a) CH3NH3I and (b) CH3NH3Cl

2.3 Synthesis of CH3NH3SnCl3 and CH3NH3ISnCl2

Equimolar CH3NH3Cl and tin (II) chloride dihydrate was dissolved into N, N-dimethylformamide separately. According to stoichiometric, the prepared solution was added and the solution of CH3NH3SnCl3 (MASC) was obtained.

Similarly equimolar CH3NH3I and tin (II) chloride dihydrate was dissolved into N, N- dimethylformamide separately. The prepared solution was added and the solution of CH3NH3ISnCl2 (MAISC) was obtained.

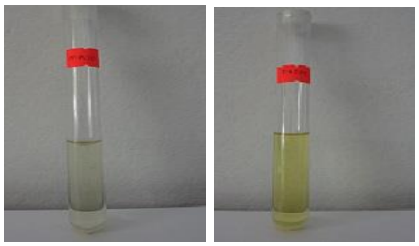

Fig. 2. Synthesized CH3NH3SnCl3 and CH3NH3ISnCl2

2.4 Film Deposition

The solution of CH3NH3SnCl3 and CH3NH3ISnCl2 was deposited onto a clean glass substrate by spin coating process at 1500 rpm for 30 seconds and then deposited film was kept at room temperature.

2.5 Characterization

The X-ray diffraction (XRD) method was used to investigate structural properties of synthesized materials determined using "GBC EMMA" XRD arrangements and for morphological structure, SEM measurement was investigated using "Evo18, curl Zeiss".

3 Results and Discussion

As demonstrated in this document, the numbering for sections upper case Arabic numerals, then upper case Arabic numerals, separated by periods. Initial paragraphs after the section title are not indented. Only the initial, introductory paragraph has a drop cap.

3.1 X-ray Diffraction (XRD)

The XRD spectra shows the peak position of synthesized MAC and MAI both in crystal and after deposition as shown in figure 3. The studies XRD pattern of crystal CH3NH3I and film deposited film by solution of CH3NH3I confirmed tetragonal structure. For crystal CH3NH3I the XRD pattern depict that the sharp peak in 2θ angle were 24.772°, 29.467°, 31.457° and 57.267°. For film the peaks analyzed in 2θ angle were, 24.772°, 30.007° and 56.984°. For both crystal and film indicates the plane (100), (110) and (211). For crystal CH3NH3Cl the XRD pattern depicts that the planes were (1 0 0), (1 1 0), (2 0 0), (3 1 0) in 2θ =17.66269°, 22.9399038°, 29.2536055° and 58.5745192°. For film the orientation was (1 0 0) in 2θ = 17.9113461° [19] [20][21].

- *Kanij Fatema is working as lecturer, department of EEE, Bangladesh University of Business and Technology (BUBT), Bangladesh, Email:kanji_fatema@bubt.edu.bd*
- *Co-Author Dr. Farid Ahmed is working as professor, department of physics, Jahangirnagar University(JU), Bangladesh, PH-01123456789. E-mail: fahmed@juniv.edu.*
(*This information is optional; change it according to your need.)*

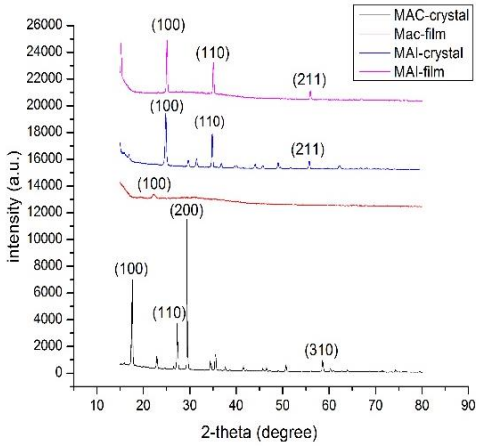

Fig. 3. XRD pattern of MAC and MAI

Figure 4 represents the XRD spectra for synthesized MASC and MAISC. The peak position of synthesized MASC are obtained at angle 2θ =11.50º, 25º and 38º which corresponds to the plane (100), (111) and (002). The peak position of synthesized MAISC are obtained at angle 2θ =20.42º and 29.98º which relates to the plane (220), and (410) [22].

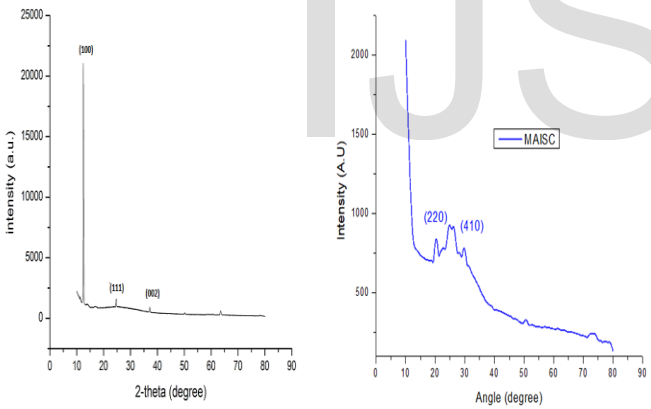

Fig. 4. XRD pattern of synthesized CH3NH3SnCl3 and CH3NH3ISnCl2

The lattice parameters of the prepared crystals were calculated via "Full Proof" software and listed in Table 1. It is observed that all the synthesized Sn-based perovskites possess a cubic crystal phase MAISC and tetragonal crystal phase for MASC with a variation in lattice parameters which is caused by the structural deformation due to the variation of halide ions stoichiometry.

TABLE 1
LATTICE PARAMETERS AND VOLUME FOR SYNTHEISZED MATERIALS

Synthesized Materials	Lattice parameters (Å) (α = β = γ = 90°)			Cell Volume (Å³)
	a	b	c	
MASC	7.64	7.64	4.73	276.76
MAISC	12.28	12.28	12.28	1852.8

The grain size of synthesized materials has been calculated from the X-ray diffraction pattern using the Debye -Scherrer equation [23].

$$\text{Crystallite size, } L = K\lambda/(\beta \cos\theta) \quad (1)$$

Where β, λ, K are full-width half-maxima, X-ray wavelength, and Scherrer constant (~0.89), respectively. The grain size 33.4 nm, 40.2 nm and 49.1 nm for synthesized MASC and 39.334 nm and 41.915 nm synthesized MAISC.

For crystalline material, dislocation density (ρ) is the measurement of number of dislocations per unit volume and can be calculated by following equation [24]-

$$\rho = 1/L\text{^}(2) \quad (2)$$

The dislocation density for MASC 0.00089 nm^{-2}, 0.00062 nm^{-2} and 0.000414 nm^{-2} and for MAISC are 0.00065 nm^{-2} and 0.00057 nm^{-2}, as demonstrated in Table 2.

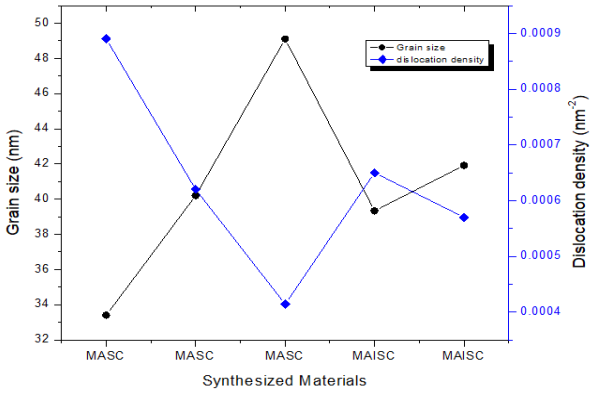

Fig. 5. Grain size and dislocation density for synthesized MASC and MAISC

The grain size is increasing and dislocation density decreasing with the shifting of peaks toward the higher value in both MASC and MAISC.

TABLE 2
GRAIN SIZE AND DISLOCATION DENSITY FOR SYNTHESIZED MASC AND MAISC

Parameters	MASC			Average	MAISC		Average
Grain size (nm)	33.4	40.2	49.1	40.9	39.334	41.915	40.62
Dislocation density (nm^{-2})	0.00089	0.00062	0.000414	0.00064	0.00065	0.00057	0.00061

3.2 Scanning Electron Microscope (SEM)

The SEM image shows some crystal growth for both MASC and MAISC as shown in figure 6. The histogram shows the irregular distribution of grain size with diameter. The average grain size are 334.68 µm for MASC and 464.88 µm for MAISC [16].

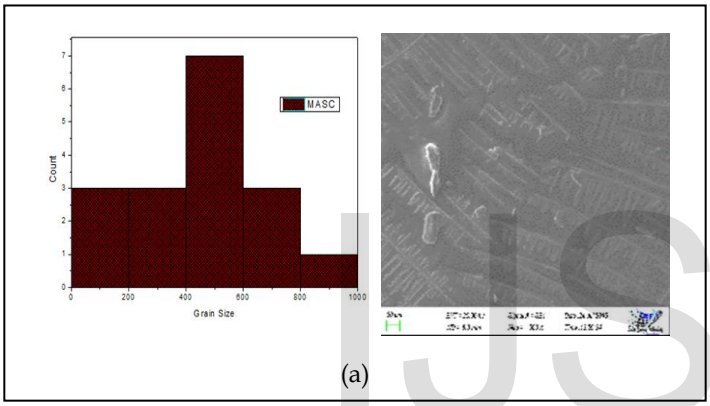

Fig. 5. SEM morphological structure of (a) CH3NH3SnCl3 and (b) CH3NH3ISnCl2

4 Conclusion

The two Sn- based perovskite materials CH3NH3SnCl3 and CH3NH3ISnCl2 are synthesized. The structural properties for both MASC and MAISC are determined by XRD. The MASC having cubic crystal phase phase (a=b=c & α = β = γ = 90°) and MAISC having tetragonal structure (a=b=c & α = β = γ = 90°). The grain size of the synthesized materials is calculated using Debye -Scherrer equation average grain size are 40.9 nm and 40.62 nm for MASC and MAISC respectively. Again, it has been observed that the grain size increasing with the shifting of peak position and dislocation density decreasing. The SEM structure shows some irregular crystal growth having average particle size ~ 334.68 µm for MASC and ~464.88 µm for MAISC.

Acknowledgment

The financial support for this research was provided by the Bangladesh Ministry of Science and Technology (MOST) through the National Science and Technology (NST) Fellowship. The authors also acknowledge M. S. Bashar, Principle Scientific Officer, Bangladesh Council of Scientific and Industrial Research, for providing necessary characterization techniques.

References

[1] [1] S. S. Mali and C. K. Hong, "p-i-n/n-i-p type planar hybrid structure of highly efficient perovskite solar cells towards improved air stability: synthetic strategies and role of p-type hole transport layer (HTL) and n-type electron transport layer (ETL) metal oxides," Nanoscale, p., 2016, doi: 10.1039/C6NR02276F.

[2] [2] S. S. Mali, C. S. Shim, and C. K. Hong, "Highly stable and efficient solid-state solar cells based on methylammonium lead bromide (CH3NH3PbBr3) perovskite quantum dots," NPG Asia Mater., vol. 7, no. 8, p. e208, 2015, doi: 10.1038/am.2015.86.

[3] [3] and M. K. N. Peng Gao*, Michael Grätzel, "Environmental Science Organohalide lead perovskites for photovoltaic applications," Energy Environ. Sci., vol. 1, no. c, pp. 2448–2463, 2012, doi: 10.1039/c4ee00942h.

[4] [4] C. H. Lu, G. V. Biesold-Mcgee, Y. Liu, Z. Kang, and Z. Lin, "Doping and ion substitution in colloidal metal halide perovskite nanocrystals," Chem. Soc. Rev., vol. 49, no. 14, pp. 4953–5007, 2020, doi: 10.1039/c9cs00790c.

[5] [5] G. E. Eperon, S. D. Stranks, C. Menelaou, M. B. Johnston, L. M. Herz, and H. J. Snaith, "Formamidinium lead trihalide: a broadly tunable perovskite for efficient planar heterojunction solar cells," Energy Environ. Sci., vol. 7, no. 3, p. 982, 2014, doi: 10.1039/c3ee43822h.

[6] [6] A. Kojima, K. Teshima, Y. Shirai, and T. Miyasaka, "Organometal halide perovskites as visible-light sensitizers for photovoltaic cells," J. Am. Chem. Soc., vol. 131, no. 17, pp. 6050–6051, 2009, doi: 10.1021/ja809598r.

[7] [7] J. H. Im, C. R. Lee, J. W. Lee, S. W. Park, and N. G. Park, "6.5% Efficient Perovskite Quantum-Dot-Sensitized Solar Cell," Nanoscale, vol. 3, no. 10, pp. 4088–4093, 2011, doi: 10.1039/c1nr10867k.

[8] [8] G. W. Kim, H. Choi, M. Kim, J. Lee, S. Y. Son, and T. Park, "Hole Transport Materials in Conventional Structural (n–i–p) Perovskite Solar Cells: From Past to the Future," Adv. Energy Mater., vol. 10, no. 8, pp. 1–30, 2020, doi: 10.1002/aenm.201903403.

[9] [9] R. Sheng et al., "Methylammonium lead bromide perovskite-based solar cells by vapor-assisted deposition," J. Phys. Chem. C, vol. 119, no. 7, pp. 3545–3549, 2015, doi: 10.1021/jp512936z.

[10] [10] J. H. Heo and S. H. Im, "Highly reproducible, efficient hysteresis-less CH3NH3PbI3-xClx planar hybrid solar cells without requiring heat-treatment," Nanoscale, vol. 3, p. DOI: 10.1039/C5NR08458J, 2016, doi: 10.1039/C5NR08458J.

[11] [11] NREL, "Cell-Pv-Eff-Emergingpv.202001042.Pdf." 2021.

[12] [12] K. Nishimura et al., "Lead-free tin-halide perovskite solar cells with 13% efficiency," Nano Energy, vol. 74, no. March, p. 104858, 2020, doi: 10.1016/j.nanoen.2020.104858.

[13] [13] P. Roy, S. Tiwari, and A. Khare, "An investigation on the influence of temperature variation on the performance of tin (Sn) based perovskite solar cells using various transport layers and absorber layers," Results Opt., vol. 4, no. March, p. 100083, 2021, doi: 10.1016/j.rio.2021.100083.

[14] [14] F. Giustino and H. J. Snaith, "Toward Lead-Free Perovskite Solar Cells," ACS Energy Lett., vol. 1, no. 6, pp. 1233–1240, 2016, doi: 10.1021/acsenergylett.6b00499.

[15] [15] K. Fatema and S. Arefin, "Enhancing the efficiency of Pb-based and Sn-based perovskite solar cell by applying different ETL and HTL using SCAPS-ID," Opt. Mater. (Amst)., vol. 125, no. February, p. 112036, 2022, doi: 10.1016/j.optmat.2022.112036.

[16] [16] N. K. Noel et al., "Lead-Free Organic-Inorganic Tin Halide Perovskites for Photovoltaic Applications," Energy Environ. Sci., vol. 7, pp. 3061–3068, 2014, doi: 10.1039/C4EE01076K.

[17] [17] E. Jokar, C. H. Chien, C. M. Tsai, A. Fathi, and E. W. G. Diau, "Robust Tin-Based Perovskite Solar Cells with Hybrid Organic Cations to Attain Efficiency Approaching 10%," Adv. Mater., vol. 31, no. 2, pp. 1–7, 2019, doi: 10.1002/adma.201804835.

[18] [18] N. J. Jeon, J. H. Noh, Y. C. Kim, W. S. Yang, S. Ryu, and S. Il Seok, "Solvent engineering for high-performance inorganic-organic hybrid perovskite solar cells.," Nat. Mater., vol. 13, no. July, pp. 1–7, 2014, doi: 10.1038/nmat4014.

[19] [19] E. L. Unger et al., "Chloride in lead chloride-derived organo-metal halides for perovskite-absorber solar cells," Chem. Mater., vol. 26, no. 24, pp. 7158–7165, 2014, doi: 10.1021/cm503828b.

[20] [20] M. Kim et al., "Methylammonium Chloride Induces Intermediate Phase Stabilization for Efficient Perovskite Solar Cells," Joule, vol. 3, no. 9, pp. 2179–2192, 2019, doi: 10.1016/j.joule.2019.06.014.

[21] [21] G. Li et al., "High detectivity photodetectors based on perovskite nanowires with suppressed surface defects," Photonics Res., vol. 8, no. 12, p. 1862, 2020, doi: 10.1364/prj.403030.

[22] [22] Y. Li et al., "50% Sn-Based Planar Perovskite Solar Cell with Power Conversion Efficiency up to 13.6%," Adv. Energy Mater., vol. 6, no. 24, pp. 1–7, 2016, doi: 10.1002/aenm.201601353.

[23] [23] M. T. Ahmed, S. Islam, and F. Ahmed, "Synthesis of (CH3NH3)2CuCl4 nanoparticles by antisolvent engineering," J. Cryst. Growth, vol. 587, Jun. 2022, doi: 10.1016/j.jcrysgro.2022.126637.

[24] [24] S. Dolabella, A. Borzì, A. Dommann, and A. Neels, "Lattice Strain and Defects Analysis in Nanostructured Semiconductor Materials and Devices by High-Resolution X-Ray Diffraction: Theoretical and Practical Aspects," Small Methods, vol. 6, no. 2, 2022, doi: 10.1002/smtd.202100932.